Macroscale Properties of Porous Media from a Network Model of Biofilm Processes

Brian J. Suchomel, Mathematics Department
University of New Hampshire, Durham, New Hampshire.

Benito M. Chen, Department of Mathematics
University of Wyoming, Laramie, Wyoming.

Myron B. Allen, Department of Mathematics
University of Wyoming, Laramie, Wyoming.

November 4, 1997

Abstract

We demonstrate how a network model can predict porosity and permeability changes in a porous medium as a result of biofilm buildup in the pore spaces. A biofilm consists of bacteria and extracellular polymeric substances (EPS) bonded together and attached to a surface. In this case, the surface consists of the walls of the porous medium, which we model as a random network of pipes.

Our model contains five species. Four of these are bacteria and EPS in both fluid and adsorbed phases. The fifth species is nutrient, which we assume to reside in the fluid phase only. Bacteria and EPS transfer between the adsorbed and fluid phases through adsorption and erosion or sloughing. The adsorbed species influence the effective radii of the pipes in the network, which affect the porosity and permeability.

We develop a technique for integrating the coupled system of ordinary and partial differential equations that govern transport of these species in the network. We examine ensemble averages of simulations using different arrays of pipe radii having identical statistics. These averages show how different rate parameters in the biofilm transport processes affect the concentration and permeability profiles.

KEYWORDS: Network models of porous media, biofilms, biobarriers.

1 Introduction

Bacterial bioremediation is a promising technique for controlling pollution in aquifers. Bacteria, already present or injected into the porous rock, either destroy the contaminant or plug the pores, forming biobarriers that restrict the spread of pollutant. We are concerned with biobarrier formation. In this process, bacteria attach to the pore walls and form biofilms by producing chains of bacteria linked by extracellular polymeric substances (EPS). The biofilms thicken and plug the medium through several processes, including the growth and attachment of bacteria and EPS. Descriptions of some lab-scale experiments that have been performed to produce biobarriers may be found in chapter 17 of Amy and Haldeman (1997) and in MacLeod et al. (1988).

To assess these effects at the macroscopic scale, we propose a network model of biofilm growth in porous media. The model incorporates microscale phenomena by treating porous media as systems of interconnected pipes, simulating the transport, reaction, and phase exchange of bacteria, EPS, and nutrients in the pipes. Detailed mathematics of the flow and transport simulation appear in Suchomel et al. (to appear). In the present work, we incorporate realistic physical and biochemical processes into that methodology to account for the effects of biofilms.

In all of the simulations presented here, we begin with a medium saturated with pure water and a small uniform amount of bacteria adsorbed to the pore walls. We model bacterial growth by allowing bacteria to consume nutrients, produce EPS, and adsorb onto the rock. The biofilm consists of adsorbed bacteria and EPS. We also allow erosion (sloughing) of the adsorbed species in response to shear forces. These processes are kinetic, with concentrations in the adsorbed and fluid phases not necessarily in local equilibrium at any instant. The amount of biomass in the adsorbed phase determines the porosity and permeability.

The paper has the following organization: In Section 2 we describe how different processes affect a porous medium at the microscopic level, then develop equations governing these processes in the pipes of a network. In Section 3 we describe a stable integration technique for these equations. In Section 4 we present results of simulations performed on ensembles of networks containing thousands of pipes, illustrating how various process parameters affect biofilm formation. Section 5 summarizes our conclusions.

2 Processes Modeled

Our model includes three species: one bacterial species, one reaction byproduct species, and one nutrient species. They can reside in either an adsorbed phase, or in the solution (fluid) phase. All of the nutrients are assumed to reside in the fluid phase. Their concentration is c_n, measured in mass per volume of fluid. Bacteria may reside in the adsorbed phase, with concentration B (mass per pore volume), or suspended in the fluid, with concentration c_b (mass per volume of fluid). The byproduct consists of long filaments of EPS. The concentration of adsorbed EPS is E (mass per pore volume), and the concentration of EPS in the fluid is c_e (mass per volume of fluid).

There are two types of biochemical reactions in our system: the conversion of nutrients into

bacterial cells, and the conversion of nutrients into EPS (see Bryers and Characklis, in Melo et al. ed. 1992). Since bacteria and EPS can reside in both the fluid and adsorbed (biofilm) phases, we write these reactions as follows:

$$\begin{aligned}
\text{nutrients} &\longrightarrow Y_B \times \text{(adsorbed bacteria)} \\
\text{nutrients} &\longrightarrow Y_b \times \text{(bacteria in fluid)} \\
\text{nutrients} &\longrightarrow Y_E \times \text{(adsorbed EPS)} \\
\text{nutrients} &\longrightarrow Y_e \times \text{(EPS in fluid).}
\end{aligned}$$

The positive factors Y_j denote the mass of species j produced by the consumption of one unit of mass of nutrients. We neglect reaction products other than bacteria and EPS. For this paper, simulations were performed with all of the $Y_j < 1$. This means that a unit mass of nutrients gets converted into less than one unit of either bacteria or EPS.

The five concentrations obey corresponding transport equations, templates for which are as follows:

$$\begin{aligned}
\frac{\partial c_n}{\partial t} + \frac{\partial}{\partial x}(\text{flux}) &= -\frac{1}{Y_b} r_{n,b} - \frac{1}{Y_e} r_{n,e} - \frac{1}{Y_B} r_{n,B} - \frac{1}{Y_E} r_{n,E}, \\
\frac{\partial c_b}{\partial t} + \frac{\partial}{\partial x}(\text{flux}) &= r_{n,b} - r_{b,B} + r_{B,b}, \\
\frac{\partial c_e}{\partial t} + \frac{\partial}{\partial x}(\text{flux}) &= r_{n,e} - r_{e,E} + r_{E,e}, \\
\frac{dB}{dt} &= r_{n,B} + r_{b,B} - r_{B,b}, \\
\frac{dE}{dt} &= r_{n,E} + r_{e,E} - r_{E,e}.
\end{aligned}$$

The terms labeled "flux," described in more detail in Section 3, account for the movement of the mobile (nonadsorbed) species with the fluid occupying the pore space. The terms on the right sides of these equations stand for exchanges due to physical and biochemical reactions:

$r_{n,b}$ = rate of creation of bacterial mass in the fluid;

$r_{n,e}$ = rate of creation of EPS mass in the fluid;

$r_{n,B}$ = rate of creation of adsorbed bacterial mass;

$r_{n,E}$ = rate of creation of adsorbed EPS mass;

$r_{b,B}$ = rate of adsorption of bacterial mass from the fluid;

$r_{e,E}$ = rate of adsorption of EPS from the fluid;

$r_{B,b}$ = rate of erosion of adsorbed bacteria from the biofilm;

$r_{E,e}$ = rate of erosion of adsorbed EPS from the biofilm.

We devote the rest of this section to a description of these terms and how they affect the flow properties of the network. The discussion occasionally refers to the flow and transport calculations, reviewed in more detail in Section 3.

2.1 Biochemical reactions

Our model allows the conversion of nutrients to either bacteria or EPS. We use Monod kinetics to describe the rate of bacterial growth as a result of the conversion of nutrient mass (Characklis and Marshall, 1990):

$$r_{n,b} = \mu_b \frac{c_n c_b}{K_s + c_n}; \qquad r_{n,B} = \mu_B \frac{c_n B}{K_s + c_n}.$$

Here, μ_b, μ_B, and K_s are positive constants.

Monod reaction kinetics exhibit the following behavior (Alexander, 1994). At low nutrient concentrations, the reaction rate is roughly proportional to the nutrient concentration. Above some relatively high concentration of nutrient, the growth rate does not increase much with increased nutrient concentration. The constant K_s represents the nutrient concentration at which the growth rate is half its maximum value.

For the production of EPS via nutrient consumption, we use a model proposed by Bryers and Characklis (Melo et al. ed. 1992):

$$r_{n,e} = \mu_e \frac{c_n c_b}{K_s + c_n}; \qquad r_{n,E} = \mu_E \frac{c_n B}{K_s + c_n}.$$

Here, μ_e and μ_E are related to the rate constants μ_b and μ_B:

$$\mu_e = k_1 \mu_b + k_1', \qquad \mu_E = k_2 \mu_B + k_2'.$$

The parameters k_1 and k_2 are growth-related constants, and k_1' and k_2' are constants not related to bacterial growth. This model assumes that any EPS produced by bacteria in the fluid goes into the fluid, and any EPS produced by adsorbed bacteria becomes part of the biofilm.

2.2 Adsorption and Erosion

Adsorption and erosion are physical processes in which bacteria and EPS migrate kinetically between the fluid and adsorbed phases. There are two separate modeling considerations associated with this migration. First, how does the mass exchange affect the radii of the pipes in the network? Second, at what rates do the exchanges occur?

To account for the effects of adsorption and erosion on pipe radii, we use volumetric considerations. In the transport model, described below and in Suchomel et al. (to appear), we divide each pipe in the network into discrete zones. The biofilm in each zone has species concentrations B and E. We assume that these species have the same density ρ_B within the biofilm. Let $B_{\mathrm{tot}} = B + E$. A mass balance allows us to compute the fluid volume of each zone after adsorption and erosion. From this information we can compute the new pipe radius, $a(t)$, and the biofilm thickness, d_{film}, in each zone.

Consider first the change in zone volume. The volume of a biofilm-free zone is

$$V(0) = \pi a^2(0)\ell, \tag{1}$$

where ℓ is the length of the zone and $a(0)$ is its biofilm-free radius. The volume of the biofilm is

$$V_{\mathrm{film}}(t) = \frac{B_{\mathrm{tot}}(t)}{\rho_{\mathrm{B}}} \pi a^2(0)\ell. \tag{2}$$

(We assume that the biofilm mass is distributed uniformly around the wall of the zone.) Subtracting equation (2) from equation (1) gives the fluid volume of the zone after adsorption:

$$V(t) = V(0) - V_{\text{film}}(t) = \pi a^2(0)\ell\left[1 - B_{\text{tot}}(t)/\rho_{\text{B}}\right].$$

Corresponding to this updated volume is a new effective radius of the zone:

$$a(t) = a(0)\sqrt{1 - B_{\text{tot}}(t)/\rho_{\text{B}}}. \tag{3}$$

The biofilm thickness in the zone is then the difference between its biofilm-free radius and its current radius,

$$d_{\text{film}}(t) = a(0) - a(t) = a(0)\left(1 - \sqrt{1 - B_{\text{tot}}(t)/\rho_{\text{B}}}\right).$$

This calculation allows different biofilm thicknesses in different zones in a pipe.

We turn now to the question of rates. Escher (1986) describes the rate of bacterial cell adsorption as first-order in the suspended cell concentration:

$$r_{b,B} = k_b c_b.$$

We model the adsorption of EPS similarly:

$$r_{e,E} = k_e c_e.$$

The factors k_b and k_e are adsorption rate constants for bacteria and EPS, respectively.

Erosion of material from the biofilm into the fluid phase results from fluid shearing and possibly other influences. We assume that the erosion rate depends is proportional to the thickness of the biofilm layer, d_{film}. We assume that erosion sheds biofilm material containing concentrations of bacteria and EPS equal to those in the biofilm. To model the erosion rates $r_{B,b}$ and $r_{E,e}$ for bacteria and EPS, respectively, we use an approach suggested by Wanner and Gujer (1986). In this approach, the erosion rate is proportional to the square of the biofilm thickness. We assume that the proportionality constant, k_{E}, is constant throughout the grid. We have

$$r_{B,b} = k_{\text{E}}\frac{B}{B_{\text{tot}}}d_{\text{film}}^2, \qquad r_{E,e} = k_{\text{E}}\frac{E}{B_{\text{tot}}}d_{\text{film}}^2.$$

2.3 Resizing Pipe Radii

As mentioned above, the growth of biofilm on the pipe walls changes the pipe radii, according to equation (3). The changes in radii effect changes in pipe conductivity and hence in the permeability of the network. To simplify the updating of flow rates in the pipes, we assume that all the biomass in each pipe is distributed uniformly along the pipe's length. Thus the concentration $\overline{B}$ of bacteria in a pipe is the arithmetic mean of the bacteria concentrations in the zones of that pipe. We compute the concentration $\overline{E}$ of EPS in the pipe similarly, and $\overline{B}_{\text{tot}} = \overline{B} + \overline{E}$. We calculate the pipe radius following the reasoning used for equation (3):

$$\overline{a}(t) = a(0)\sqrt{1 - \overline{B}_{\text{tot}}(t)/\rho_{\text{B}}}. \tag{4}$$

We use these new radii to determine the pipe conductivities when solving the flow equation, a procedure described in more detail below.

This model is plausible for species of bacteria that colonize uniformly in space, such as *Pseudomonas aeruginosa* (Characklis and Marshall, 1990). The assumption of uniform growth along pipes may not be valid for bacteria that form aggregated colonies. For such cases the calculation of pipe conductivities may require an expression for flow capacity through pipes with variable cross section.

2.4 Changes in Permeability

In a network model of porous media, decreases in macroscopic permeability result from the constriction of pipes in the network. Experiments with biofilms in soil columns (Taylor and Jaffé, 1990) corroborate this picture, showing that permeability varies with both time and position as biofilm develops. An important goal of our modeling work, explored in Section 4, is to examine the effects that microscopic pipe constrictions have on macroscopic permeability.

In a network model, we can compute the permeability associated with individual layers of pipes — a feat whose analog is difficult to accomplish in laboratory column studies. For this purpose, a layer in the network consists of all junctions in a column at the same distance from the inlet side of the grid, all junctions that are connected to those junctions, and all pipes connecting those junctions. Figure 1 shows a typical layer. The permeability of a layer corresponds physically to the average permeability at a given depth in the column.

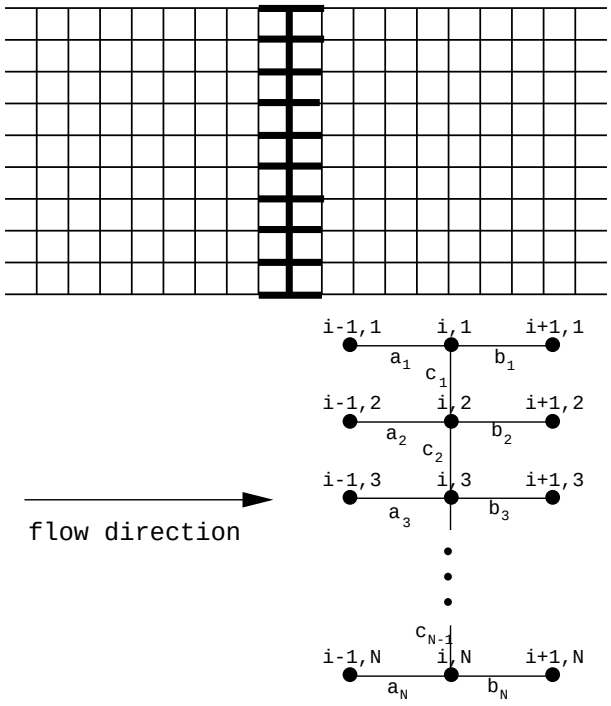

Figure 1: A sample layer in a two-dimensional grid.

To calculate the permeability of a layer i, we isolate it from the rest of the network, assigning the pressure head 0 to the junctions in column $i+1$ and a pressure head ΔH to the junctions in column $i-1$. Using the flow model described in the next section, we calculate the total flow

rate $Q_i(t)$ at time t through the layer as the sum of the flow rates into the junctions in column $i+1$. Dividing $Q_i(t)$ by ΔH gives the permeability of the layer. In displaying the results, we plot normalized permeabilities, computed relative to values at $t = 0$:

$$k_i(t) = \frac{Q_i(t)/\Delta H}{Q_i(0)/\Delta H}.$$

Similarly, we calculate the flow $Q(t)$ through the whole network as the sum of the flow rates into the junctions on the outlet side of the network. Then the normalized permeability of the network is

$$\frac{Q(t)/\Delta H}{Q(0)/\Delta H},$$

where ΔH is now the pressure head drop across the entire network.

2.5 Changes in Porosity

The porosity of a porous medium also changes as biofilm grows and clogs the pore spaces. Porosity (Scheidegger, 1957) is the ratio of void space to total volume (void space + rock volume). In a network model, the volume inside the pipes represents the void space. We make no effort to represent the rock volume in our model (although one could do so arbitrarily). Instead, we calculate a normalized porosity relative to the initial pipe volume in the network.

To examine how porosity changes at different depths, we divide the network into layers. The layers used to compute porosity are similar to those used in calculating permeability, with a slight variation. Consider first a single pipe. At this scale, the normalized porosity is the ratio of the current volume to the initial volume in the pipe. Since pipe lengths do not change, the normalized porosity $\eta(t)$ is just the ratio of the cross sectional area at time t to that at time 0 or, equivalently, $\eta(t) = a^2(t)/a^2(0)$.

The normalized porosity of a layer is a straightforward extension. We define a layer as the set of all pipes connecting the junctions in one column, along with half of each pipe connecting these to junctions in other columns. In Figure 1, layer i contains all of the pipes labeled c_k for $k = 1, \ldots, N-1$ and half of each of the pipes labeled a_k and b_k for $k = 1, \ldots, N$. To calculate the void volume in layer i, let $Z_{i,j}$ be the number of pipes connected to junction i, j, and let $a_{i,j,k}$ be the radius of the kth pipe connected to this junction and let $\ell_{i,j,k}$ be the length of that pipe. Then the void volume of layer i is

$$\frac{1}{2} \sum_{j=1}^{N-1} \sum_{k=1}^{Z_{i,j}} \ell_{i,j,k} a_{i,j,k}^2.$$

Dividing by the initial void volume gives the normalized porosity of the layer, which we call $\hat{\phi}_i$. We compute the normalized porosity of the network similarly, computing the total void space in the network as the total volume of the pipes.

3 Simulation Technique

Our model includes three types of physical processes. The first is flow through the porous medium, which involves computing fluid velocities in all of the pipes in the network. The second is transport

of solutes through the pipes by advection and diffusion. The third type of process includes the physical and biochemical exchanges described in Section 2. There are several types of coupling among these processes. Fluid velocities determined by the flow physics obviously affect the solute transport. In turn, transport influences the concentrations of nutrients and biomass available for reaction and adsorption. The adsorbed concentrations affect local permeabilities, which influence the flow equation.

This section briefly describes the numerics used to model these phenomena. In the case of flow and transport, further details of the model appear in Suchomel et al. (to appear). In the case of biofilm processes, the following discussion includes a complete description.

3.1 Discretizing Flow and Transport

We model the pore spaces in a porous medium as a set of interconnected pipes arranged in a regular network, with no volume associated with the pipe junctions. The initial radii of the pipes are random, assigned according to a lognormal probability distribution. No distinction is made when assigning radii among pipes oriented in different directions. This results in an isotropic medium. Fluid flow through the pipes obeys the Hagen-Poiseuille equation: If $q_{i,j}$ denotes the volumetric flow rate in the pipe connecting junction i to junction j in the network, then

$$q_{i,j} = \hat{k}\,(h_j - h_i)\,. \tag{5}$$

Here $\hat{k} = \rho g \pi a^4/(8\mu\ell)$, where a is the pipe radius, ρ and μ are the density and viscosity of the fluid, g is the acceleration of gravity, and ℓ is the length of the pipe. The symbols h_i and h_j denote the pressure head at junctions i and j, respectively.

Given a pressure head difference across the ends of the network, we solve for the flow rate through each pipe using equation (5). The requirement that the flow rates at any junction sum to zero yields a sparse, symmetric, positive definite linear system for the pressure head values at the interior junctions of the network. We solve this system via an iterative scheme. Then, using the pressure head values, we compute volumetric flow rates via equation (5).

Biofilm growth changes the flow in the network. In principle, we should re-solve the flow equation as we update biofilm growth. However, when this growth is slow compared with the time scales of transport, the flow properties of the network do not change rapidly. In this case, we assume that fluid velocities remain approximately constant over several time steps. This assumption permits considerable computational savings, since each update of the flow equation requires the iterative solution of a large linear system.

We consider transport to be a one-dimensional process in each pipe. This process involves both advection with the mean velocity in each pipe and diffusion along the pipe's axis. First consider advection. The mean velocity is the volumetric flow rate divided by the cross sectional area:

$$\bar{v} = q/(\pi a^2). \tag{6}$$

To discretize advection, we partition each pipe into zones using a spatial grid. Thus we solve transport equations on a discretization that is finer than the one used to solve the flow equation. Since many pipes may meet at a junction of the network, we compute boundary concentrations for individual pipes as flow-weighted averages of other pipes intersecting the junction. We use an

upwind explicit finite-difference discretization of advection on the grid in each pipe, as described in more detail below.

For visualization purposes, it is too costly to plot concentrations at each zone in the transport grid. Instead, we plot concentrations on the network used in solving the flow equation. We also show one-dimensional concentration plots, which display areally averaged concentrations versus depth. This device is especially useful in three-dimensional simulations, where visualization is otherwise difficult. Suchomel et al. (to appear) discuss further details of the transport and visualization algorithms.

3.2 Equations Governing Transport

To obtain specific transport equations for the five components in our model, we substitute detailed expressions for the flux and exchange terms in the template equations presented in Section 2. For the mobile species (nutrients, bacteria, and EPS suspended in the fluid), we assume that the advective velocity is the fluid velocity $\bar{v}$ and that there is a Fickian diffusion term, with a common diffusion coefficient D, that accounts for the spread of individual species with respect to $\bar{v}$. Thus the flux terms have the form

$$\frac{\partial}{\partial x}(\text{flux}) = \bar{v}\frac{\partial c_i}{\partial x} - D\frac{\partial^2 c_i}{\partial x^2}.$$

(We assume that D is a small constant, and by construction $\bar{v}$ is constant within each pipe.) We discuss diffusion in the next section and near the end of section 4.

For the exchange terms $r_{n,b}, r_{n,e}, r_{n,B}, r_{n,E}, r_{b,B}, r_{e,E}, r_{B,b}, r_{E,e}$, we substitute the expressions developed in Section 2. Thus we have the following transport equations: For nutrients,

$$\begin{aligned}\frac{\partial c_n}{\partial t} &= D\frac{\partial^2 c_n}{\partial x^2} - \bar{v}\frac{\partial c_n}{\partial x} - \left(\frac{\mu_b}{Y_b} + \frac{k_1\mu_b + k_1'}{Y_e}\right)\frac{c_n c_b}{K_s + c_n} \\ &\quad - \left(\frac{\mu_{\mathrm{B}}}{Y_B} + \frac{k_2\mu_{\mathrm{B}} + k_2'}{Y_E}\right)\frac{c_n B}{K_s + c_n}.\end{aligned} \tag{7}$$

For bacteria in the fluid,

$$\frac{\partial c_b}{\partial t} = D\frac{\partial^2 c_b}{\partial x^2} - \bar{v}\frac{\partial c_b}{\partial x} + \left(\mu_b\frac{c_n}{K_s + c_n} - k_b\right)c_b + k_{\mathrm{E}}\frac{B}{B_{\mathrm{tot}}}d_{\mathrm{film}}^2. \tag{8}$$

For EPS in the fluid,

$$\frac{\partial c_e}{\partial t} = D\frac{\partial^2 c_e}{\partial x^2} - \bar{v}\frac{\partial c_e}{\partial x} + (k_1\mu_b + k_1')\frac{c_n c_b}{K_s + c_n} - k_e c_e + k_{\mathrm{E}}\frac{E}{B_{\mathrm{tot}}}d_{\mathrm{film}}^2. \tag{9}$$

For adsorbed bacteria,

$$\frac{dB}{dt} = \left[\mu_{\mathrm{B}}\frac{c_n}{K_s + c_n} - \frac{k_{\mathrm{E}}d_{\mathrm{film}}^2}{B_{\mathrm{tot}}}\right]B + k_b c_b. \tag{10}$$

For adsorbed EPS,

$$\frac{dE}{dt} = (k_2\mu_{\mathrm{B}} + k_2')\frac{c_n B}{K_s + c_n} - k_{\mathrm{E}}\frac{E}{B_{\mathrm{tot}}}d_{\mathrm{film}}^2 + k_e c_e. \tag{11}$$

It is possible to summarize the transport equations in vector form. Define $\mathbf{u} = (c_n, c_b, c_e)^T$, and let $\mathbf{w} = (B, E)^T$. The vector $\mathbf{u}$ of mobile species concentrations obeys an equation of the form

$$\frac{\partial \mathbf{u}}{\partial t} = D\frac{\partial^2 \mathbf{u}}{\partial x^2} - \bar{v}\frac{\partial \mathbf{u}}{\partial x} + \mathbf{f}_{1,r}(\mathbf{u}, \mathbf{w}) + \mathbf{f}_{1,s}(\mathbf{u}, \mathbf{w}), \tag{12}$$

where the vector $\mathbf{f}_{1,r}(\mathbf{u},\mathbf{w})$ contains reaction terms and $\mathbf{f}_{1,s}(\mathbf{u},\mathbf{w})$ contains adsorption and erosion terms. Similarly, the vector $\mathbf{w}$ of immobile (biofilm) species concentrations obeys an ordinary differential equation of the form

$$\frac{d\mathbf{w}}{dt} = \mathbf{f}_{2,r}(\mathbf{u},\mathbf{w}) + \mathbf{f}_{2,s}(\mathbf{u},\mathbf{w}). \tag{13}$$

The functions $\mathbf{f}_{1,r}$, $\mathbf{f}_{1,s}$, $\mathbf{f}_{2,r}$, and $\mathbf{f}_{2,s}$ contain the nonlinear coupling among the equations:

$$\mathbf{f}_{1,r} = \begin{bmatrix} -\left(\frac{\mu_b}{Y_b} + \frac{k_1\mu_b + k_1'}{Y_e}\right)\frac{c_n c_b}{K_s + c_n} - \left(\frac{\mu_{\mathrm{B}}}{Y_B} + \frac{k_2\mu_{\mathrm{B}} + k_2'}{Y_E}\right)\frac{c_n B}{K_s + c_n} \\ \mu_b \frac{c_n c_b}{K_s + c_n} \\ (k_1\mu_b + k_1')\frac{c_n c_b}{K_s + c_n} \end{bmatrix},$$

$$\mathbf{f}_{1,s} = \begin{bmatrix} 0 \\ -k_b c_b + k_{\mathrm{E}}\frac{B}{B_{\mathrm{tot}}} d_{\mathrm{film}}^2 \\ -k_e c_e + k_{\mathrm{E}}\frac{E}{B_{\mathrm{tot}}} d_{\mathrm{film}}^2 \end{bmatrix},$$

$$\mathbf{f}_{2,r} = \begin{bmatrix} \mu_{\mathrm{B}}\frac{c_n B}{K_s + c_n} \\ (k_1\mu_{\mathrm{B}} + k_1')\frac{c_n B}{K_s + c_n} \end{bmatrix}, \qquad \mathbf{f}_{2,s} = \begin{bmatrix} k_b c_b - k_{\mathrm{E}}\frac{B}{B_{\mathrm{tot}}} d_{\mathrm{film}}^2 \\ k_e c_e - k_{\mathrm{E}}\frac{E}{B_{\mathrm{tot}}} d_{\mathrm{film}}^2 \end{bmatrix}.$$

3.3 Integrating the Transport Equations

To solve the transport equations numerically, we use a finite-difference approximation to the one-dimensional transport problem in each pipe. We use an upwind explicit finite-difference scheme to discretize the advection terms. This scheme is numerically diffusive. We use the numerical diffusion to represent physical diffusion in the pipes, arguing that it should be as small as feasible, as discussed below.

Define the operators L and L_h by

$$L\mathbf{u} = \frac{\partial \mathbf{u}}{\partial t} - D\frac{\partial^2 \mathbf{u}}{\partial x^2} + \bar{v}\frac{\partial \mathbf{u}}{\partial x},$$

and

$$L_h\mathbf{u} = \frac{\mathbf{u}_i^{n+1} - \mathbf{u}_i^n}{\Delta t} + \bar{v}\frac{\mathbf{u}_i^n - \mathbf{u}_{i-1}^n}{\Delta x}.$$

Taylor-expansion arguments show that $L_h\mathbf{u}$ approximates $L\mathbf{u}$ up to order $\mathcal{O}((\Delta x + \Delta t)^2)$ and produces numerical diffusion with diffusion coefficient D given by

$$D = \frac{\bar{v}\Delta x(1-\lambda)}{2},$$

where $\lambda = \bar{v}\Delta t/\Delta x$.

Let $N_c = \ell/\Delta x$ be the number of zones in a given pipe. As discussed in the next subsection, N_c may change as biofilm accumulates in the pipe and affects the fluid flow there. To control numerical diffusion, we typically want N_c to be as large as possible while still satisfying $N_c = \ell\lambda/(\bar{v}\Delta t) \leq \ell/(\bar{v}\Delta t)$. Since $\bar{v}$ may become small when biofilm clogs the pipe, it is necessary in practice to set an upper bound on N_c.

Equation (12) can be written as $L\mathbf{u} = \mathbf{f}_1$, where $\mathbf{f}_1 = \mathbf{f}_{1,r} + \mathbf{f}_{1,s}$. The discrete approximation to equation (12) is thus $L_h\mathbf{u} = \mathbf{f}_1$. Rearranging this approximation yields

$$\mathbf{u}_i^{n+1} = \lambda\mathbf{u}_{i-1}^n + (1-\lambda)\mathbf{u}_i^n + \mathbf{f}_1(\mathbf{u}_i^n, \mathbf{w}_i^n)\Delta t. \tag{14}$$

Physically, all concentrations are nonnegative. Computationally, it is necessary to impose this condition to keep concentration values in the ranges where the reaction terms are valid. A concentration that is nonnegative at the start of a time step may become negative at the end of a time step due to numerical effects; in particular, this can happen if the time step is too large. The following approach prohibits negative concentrations.

In Equation (14), the only entry in the reaction term $\mathbf{f}_{1,r}$ that can be negative is the one corresponding to nutrient concentrations. We isolate the reaction from the transport via an operator splitting. First we solve for the mobile species at a nominal "time level" $n + \frac{1}{2}$ using transport only:

$$\mathbf{u}_i^{n+1/2} = \lambda\mathbf{u}_{i-1}^n + (1-\lambda)\mathbf{u}_i^n, \tag{15}$$

where the subscripts index zones in the transport grid. The concentrations $\mathbf{u}^{n+1/2}$ remain nonnegative provided $\lambda \leq 1$. At level $n + \frac{1}{2}$ there is no change in adsorbed concentrations.

After integrating the transport terms in this way, we calculate an intermediate nutrient reaction rate using $\mathbf{u}^{n+1/2}$ and $\mathbf{w}^n$:

$$r_{n_i}^{n+1/2} = \left(\frac{\mu_b}{Y_b} + \frac{k_1\mu_b + k_1'}{Y_e}\right)\frac{c_{n_i}^{n+1/2}c_{b_i}^{n+1/2}}{K_s + c_{n_i}^{n+1/2}} + \left(\frac{\mu_B}{Y_B} + \frac{k_2\mu_B + k_2'}{Y_E}\right)\frac{c_{n_i}^{n+1/2}B_i^n}{K_s + c_{n_i}^{n+1/2}}.$$

The reactions $\mathbf{f}_{1,r}$ deplete nutrient concentrations and enhance all other concentrations. To guarantee that nutrient concentrations remain nonnegative during each time step, we limit these reactions. Define φ as follows:

$$\text{If} \quad c_{n_i}^{n+1/2} \geq r_{n_i}^{n+1/2}\,\Delta t, \qquad \text{then} \quad \varphi = 1.$$

$$\text{If} \quad c_{n_i}^{n+1/2} < r_{n_i}^{n+1/2}\,\Delta t, \qquad \text{then} \quad \varphi = \frac{c_{n_i}^{n+1/2}}{r_{n_i}^{n+1/2}\,\Delta t}.$$

The reaction-limited scheme for updating nutrient concentration is then

$$c_{n_i}^{n+1} = c_{n_i}^{n+1/2} - \varphi\; r_{n_i}^{n+1/2}\;\Delta t.$$

The case $\varphi = 1$ corresponds to the case when the unmodified updating scheme yields physically acceptable, nonnegative nutrient concentrations at the end of the time step. When $\varphi \neq 1$, the reaction rate would cause nutrient concentrations to be negative if we allowed it to act over the entire time step. Instead, we allow the reaction to deplete the nutrient but not to yield nonphysical concentration values. In this case, we also modify equations (12) and (13) to insure that the increases in bacteria and EPS concentrations balance the decreases in nutrient concentration.

The overall scheme proceeds as follows. First, integrate the transport terms for the mobile species using equation (15). Then compute φ and integrate the remaining reaction and adsorption terms:

$$\mathbf{u}_i^{n+1} = \mathbf{u}_i^{n+1/2} + \left[\varphi \mathbf{f}_{1,r}(\mathbf{u}_i^{n+1/2}, \mathbf{w}_i^n) + \mathbf{f}_{1,s}(\mathbf{u}_i^{n+1/2}, \mathbf{w}_i^n)\right] \Delta t$$

and

$$\mathbf{w}_i^{n+1} = \mathbf{w}_i^n + \left[\varphi \mathbf{f}_{2,r}(\mathbf{u}_i^{n+1/2}, \mathbf{w}_i^n) + \mathbf{f}_{2,s}(\mathbf{u}_i^{n+1/2}, \mathbf{w}_i^n)\right] \Delta t.$$

For example, the updating scheme for bacteria in the fluid is

$$c_{b_i}^{n+1} = c_{b_i}^{n+1/2} + \left[\varphi \ \mu_b \ \frac{c_{n_i}^{n+1/2} c_{b_i}^{n+1/2}}{K_s + c_{n_i}^{n+\frac{1}{2}}} - k_b \ c_{b_i}^{n+1/2} + k_E \frac{B_i^n}{B_{\mathrm{tot}_i}^n} \left(d_{b_i}^n\right)^2 \right] \ \Delta t,$$

while that for EPS in the biofilm is

$$E_i^{n+1} = E_i^n + \left[\varphi \ (k_2 \mu_B + k_2') \frac{c_{n_i}^{n+1/2} E_i^n}{K_s + c_{n_i}^{n+1/2}} + k_e \ c_{e_i}^{n+1/2} - k_E \frac{E_i^n}{B_{\mathrm{tot}_i}^n} \left(d_{b_i}^n\right)^2 \right] \ \Delta t.$$

The adsorption and erosion terms $\mathbf{f}_{1,s}$ and $\mathbf{f}_{2,s}$ also have the potential to produce negative concentrations. The function $\mathbf{f}_{1,s}$ contains negative terms that represent the loss of bacteria and EPS from the fluid phase due to adsorption. To guarantee that

$$\mathbf{u}_i^{n+1/2} + \mathbf{f}_{1,s}(\mathbf{u}_i^{n+1/2}, \mathbf{w}_i^n) \Delta t$$

has no negative entries, we insist that $k_b \Delta t \leq 1$ and $k_e \Delta t \leq 1$.

The only negative terms in $\mathbf{f}_{2,s}$ are those that model erosion of mass from the biofilm. To maintain nonnegative concentrations in the biofilm, we demand that no more biomass be eroded from the surface during a time step than resides on the surface at the beginning of the time step. Specifically,

$$B_{\mathrm{tot}} - k_{\mathrm{E}} d_{\mathrm{film}}^2 \Delta t = B_{\mathrm{tot}} - k_{\mathrm{E}} a^2(0) \left(1 - \sqrt{1 - \frac{B_{\mathrm{tot}}}{\rho_{\mathrm{B}}}}\right)^2 \Delta t \geq 0, \tag{16}$$

in all pipes in the network. This is a complicated inequality that involves pipe radii and biofilm density and concentration. It may be violated when Δt and B_{tot} are large, especially when some pipe has a large radius or a small biofilm density. Let $a_{\max}(t)$ denote the largest pipe radius in the network at time t. We avoid negative concentrations by choosing Δt to satisfy

$$\Delta t \leq \frac{\rho_{\mathrm{B}}}{a_{\max}^2(t) k_{\mathrm{E}}}.$$

The model executes the calculations described in this subsection at every time level.

3.4 Integrating the Flow Equation

We do not necessarily solve the flow equation at every time step. In fact, if biofilm never accumulates in the pipes, then we need only solve the flow equation once, at the beginning of a simulation. More generally, the accumulation of biofilm in the pipes often affects the fluid flow patterns on time scales larger than those characteristic of the transport.

Before solving the flow equation, we calculate new pipe radii using equation (4). After solving the flow equation again for pressure head values at the interior junctions, we compute new volumetric flow rates through individual pipes using equation (5). Then we compute mean velocities in the pipes using equation (6).

As suggested earlier, the results of re-solving the flow equation can affect the discretization of the transport equations. For example, changes in flow rates may require changing flow directions in certain pipes or a repartitioning of pipes. Since fluid flows from higher values of pressure head to lower ones, it is easy to determine whether the flow direction in a pipe has changed. When the direction changes in a given pipe, we renumber its zones by swapping the order of the concentrations. When biofilm accumulation forces a change in the number of zones in a pipe, we transfer the concentrations from the old zones to the new zones via a mass balance argument. Suchomel et al. (to appear) supply more detail.

4 Computational Results

We present results of simulations intended to model actual and possible laboratory experiments involving biofilm growth in soil columns. Among the experiments of interest are those reported by Vandevivere and Baveye (1992) and Taylor and Jaffé (1990). These simulations demonstrate that the model can reasonably mimic observed biofilm behavior in porous media, and they suggest avenues for further experiments to investigate biobarrier process design.

Starting at $t = 0$ the water flowing into the network contains nutrients at unit concentration. The bacteria consume the nutrients, growing and producing EPS. Some of the biofilm erodes and advects downstream while some remains attached to the rock. Our objective is to find changes in permeability and porosity, under various choices of process parameters, as the flow, transport, and reactions evolve. Of particular interest are parameter configurations that can produce biobarriers.

We examine simulations in two and three space dimensions. For the two-dimensional simulations, we use a 60×40 rectangular network containing 4622 pipes. We examine three-dimensional simulations on a $20 \times 15 \times 15$ rectangular network containing 11,835 pipes. These networks are large enough to reveal spatial trends but small enough to allow simulation times ranging between five minutes and two hours on an SGI Crimson. In all cases, pipe radii obey a lognormal probability distribution with a mean of 1 and a standard deviation of 0.6.

All of the results presented below assume a constant volumetric flow rate through the network, consistent with column experiments reported by Lindqvist et al. (1994), Taylor and Jaffé (1990), and Mitchell (1978). Under these conditions, clogging of some pores in the medium forces higher flow rates through others. (If, instead, we held the pressure drop through the network constant, selective pore clogging would not necessarily cause increased flow rates in other pores. This scenario may be more appropriate in simulating field experiments. Our model can operate in either mode.)

4.1 The Base Case

We first establish a base case in both two and three dimensions. The aim here is to match some of the results in the published experiments cited above. We use stoichiometric coefficients similar to

those in reported in Bakke et al. (1984), choosing the other parameters to match the experiments (see Appendix A).

The two-dimensional concentration profiles in figure 2, generated from a single simulation of the base case, illustrate the type of results that the model generates in one run. Figure 3 shows average values from 20 different runs, all of which have the same input parameters except that they use different realizations of the same lognormal distribution of pipe radii.

Tables 1 and 2 serve as a legend for all of the plots in this section. The plots labeled NC, BC, EC, BA and EA correspond to concentrations c_n, c_b, c_e, B, and E, respectively. In all of these plots the x-axis corresponds to distance from the inlet side of the grid, measured in pipe lengths and the y-axis is concentration. The plots labeled perm and poro show how normalized permeability and porosity, respectively, vary with time and space The plots labeled per2 show how the network permeability varies with time. The per2 plots have an x-axis corresponding to time, which is different than in all the other plots. The plot biofilm conc displays the total adsorbed biomass, $B + E$.

label in plots	label in text	quantity	plot style	elapsed time
NC	c_n	conc. of nutrients in sol'n	—	t = 100
BC	c_b	conc. of bacteria in sol'n	- - -	t = 200
EC	c_e	conc. of EPS in sol'n	- · - · -	t = 300
BA	B	conc. of adsorbed bacteria	· · ·	t = 400
EA	E	conc. of adsorbed EPS	• • •	t = 500
biofilm conc	$B_{\text{tot}} = B + E$	biofilm concentration		

Table 1: Description of symbols in concentration plots. In all of the plots, the x-axis is distance from the inlet and the y-axis is concentration.

label in plots	x-axis	y-axis	plot style	elapsed time
perm	distance from inlet	$(K/K_0)_i$	—	t = 50, 250, 450
poro	distance from inlet	$\hat{\phi}_i$	- - -	t = 100, 300, 500
per2	time	$(K/K_0)_{\text{grid}}$	- · - · -	t = 150, 350
			· · ·	t = 200, 400

Table 2: Description of symbols in flow properties plots.

At early times, nutrients move through the network much as they would in the absence of bacteria. As time progresses, the bacteria concentration increases to a level at which they consume most of the nutrients. At $t = 500$ a large fraction of the pipes near the inlet are clogged, and fluid containing nutrients is forced through the remaining channels at higher velocities.

Figure 3 shows the other corresponding concentrations along with porosity and permeability profiles. The porosity and permeability decrease as concentrations of EPS and bacteria in the biofilm increase. Most of the biomass resides in the adsorbed phase, reflecting the fact that the adsorption rates are large and the erosion rates are small. Concentrations of bacteria are higher

than those of EPS because reaction rate constants favor the production of bacteria.

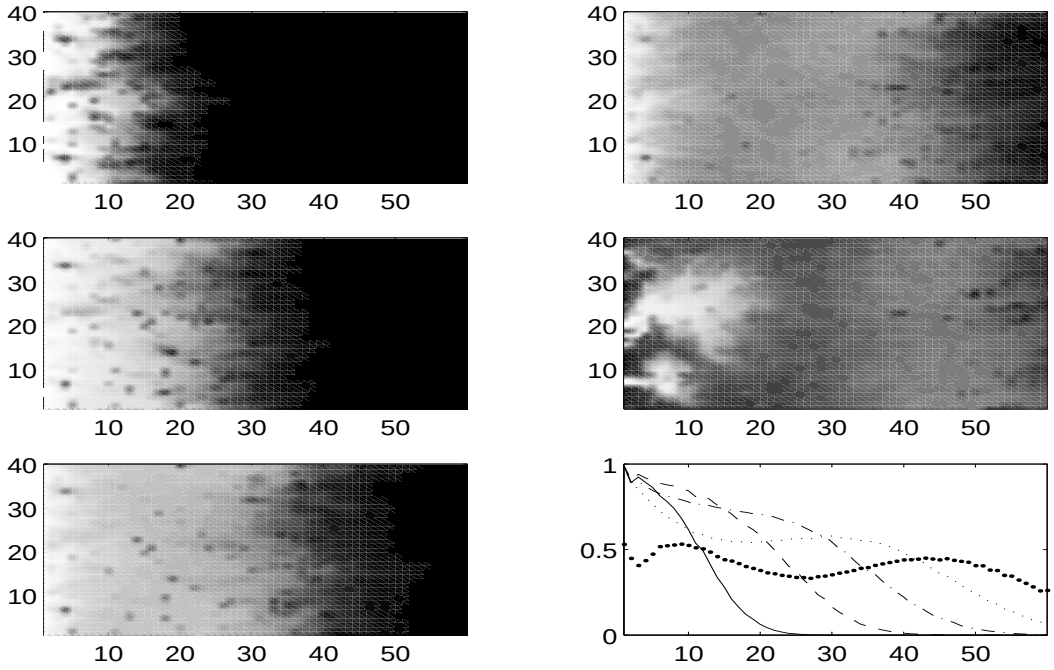

Figure 2: Nutrient concentrations for two-dimensional base case. Gray-scale plots show concentrations of a single simulation at times t=100, 200, ...,500. Black corresponds to a concentration of 0 and white corresponds to a concentration of 1. The line plot shows averages of 20 simulations.

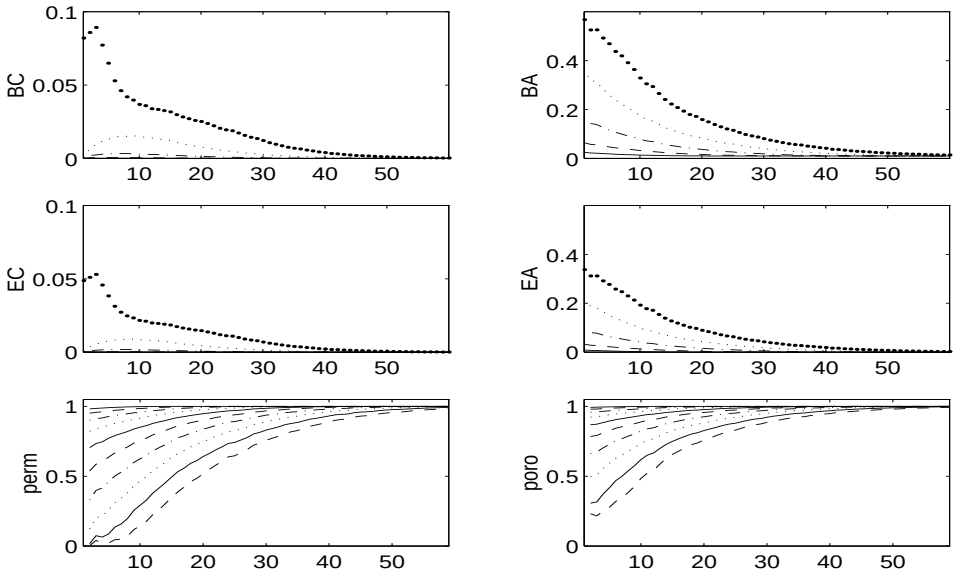

Figure 3: Concentration profiles for base case for two-dimensional simulations.

Figure 4 shows mean concentrations versus distance from the inlet for the three-dimensional

base case. All parameters are the same as for the two-dimensional base case except for the total volumetric flow rate, which is larger because a cross section of this network contains more pipes than in the two-dimensional case. The bottom row of plots compares nutrient concentrations to those obtained when no bacteria are present. Figure 5 shows the corresponding changes in porosity and permeability.

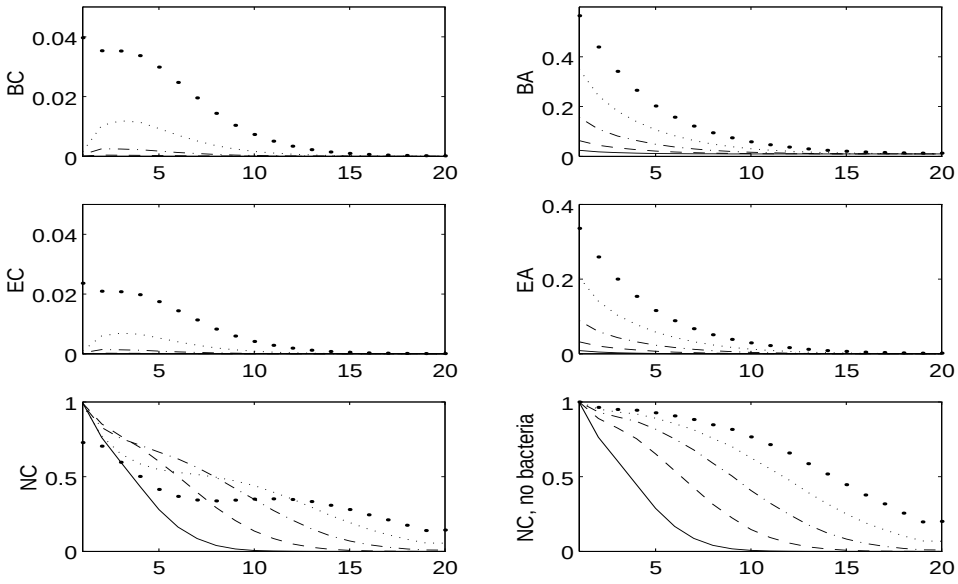

Figure 4: Base-case concentration profiles for three-dimensional simulations.

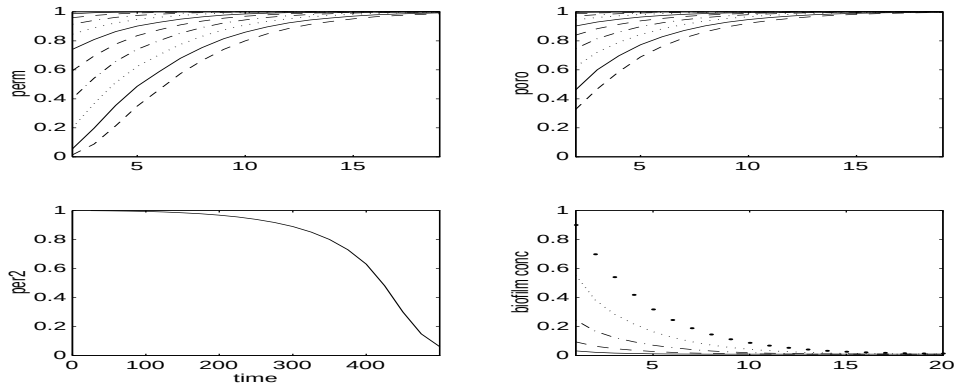

Figure 5: Changes in flow properties of medium for the three-dimensional base case.

The overall behavior is similar to that for the two-dimensional simulations. But there is a larger decrease in permeability relative to the decrease in porosity for the three-dimensional simulations than for the two-dimensional simulations. We attribute this seemingly counterintuitive result to geometric differences in the two- and three-dimensional networks. In both networks, pipes are oriented either parallel to the overall flow direction or perpendicular to it. In three dimensions, a larger fraction of the pipes are oriented perpendicular to the overall flow. Specifically, in our three-

dimensional network, 7560 out of 11,835 pipes are perpendicular to flow, while in two dimensions the corresponding ratio is 2262 out of 4622. Since flow rates are usually larger in pipes parallel to the overall flow direction, we expect more nutrients to flow through them, enhancing bacterial growth there. Clogging of these pipes also has a greater effect on the permeability than clogging of the perpendicular pipes. Hence we see a larger discrepancy between normalized porosity and normalized permeability in the three-dimensional simulations.

This reasoning suggests the investigation of different network geometries. Using Voronoi tesselations, Jerauld et al. (1984a,b) conclude that flow properties derived on regular networks differ little from those derived on random networks, provided the average coordination numbers are the same. However, our simulations suggest that, if reactions alter the flow properties over time, then networks can exhibit behavior peculiar to their geometry. This idea deserves further inquiry. Koplik (1982) lists a number of different geometries for two-dimensional networks. It may be that some regular network geometries exhibit the behavior described above while others do not, or maybe regular geometries are not appropriate for describing porous media when reaction and adsorption change the pore radii.

For the remainder of this paper, we present results of three-dimensional simulations only. Results for two-dimensional simulations were found to be similar in each of the three cases.

4.2 Case A: Effects of Adsorption and Erosion Rates

Next, we look at how simulation results vary as we change process parameters. In case A, we decrease the bacterial adsorption rate k_b, while keeping the EPS adsorption rate k_e fixed and increasing the erosion rate k_{E}. We expect more bacteria to remain in solution and to be advected downstream. Figure 6 shows concentration profiles at five different time levels, with nutrient concentrations from the base case shown in the lower right for comparison. The concentrations of bacteria and EPS are higher in solution than in the adsorbed phase, as expected. The bacteria move further downstream than in the base case, adsorbing as they travel. The permeability of the medium does not drop as much as in the base case, and the largest decrease occurs downstream of the inlet. The base case exhibits a local peak in nutrient concentrations near $x = 12$. The fluid in the base case moves past the inlet before bacteria concentration becomes high there. Thus, as more of the bacteria advect downstream, more nutrients are consumed as they pass through the network. There is a smaller decrease in permeability, because the biofilm is spread out over the length of the network and not concentrated near the inlet as in the base case.

The model predicts other effects that are reasonable but that may not be obvious a priori. The highest concentrations of bacteria at the end of a simulation occur near the middle of the network, reflecting the fact that bacteria are advecting further downstream as they consume nutrients. There is a correspondingly lower concentration of nutrients downstream. There is also a higher concentration of EPS downstream, even though the EPS adsorption rate is the same as in the base case. This downstream increase is attributable to the fact that the EPS reaction rate is proportional to the concentration of advected bacteria.

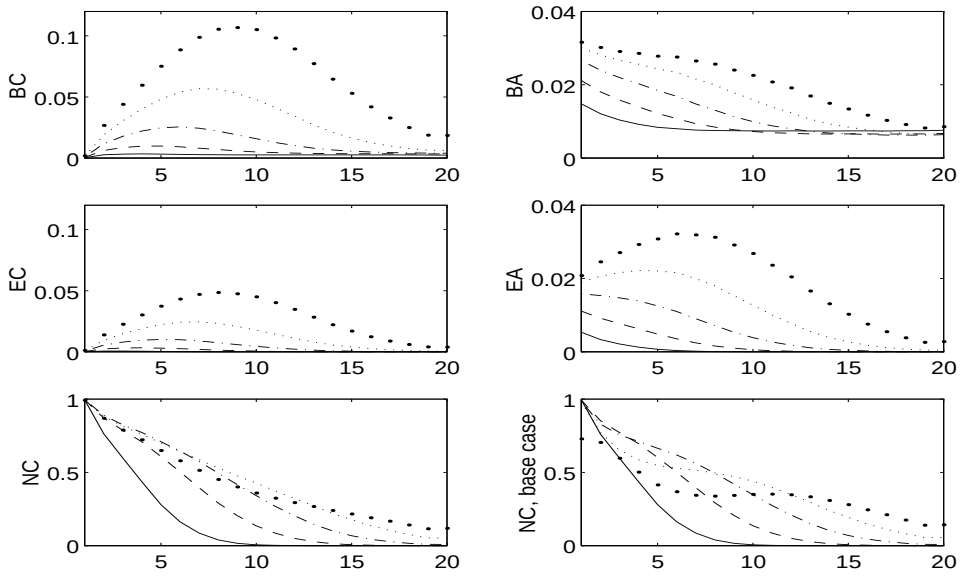

Figure 6: Concentration profiles for case A for three dimensional simulations.

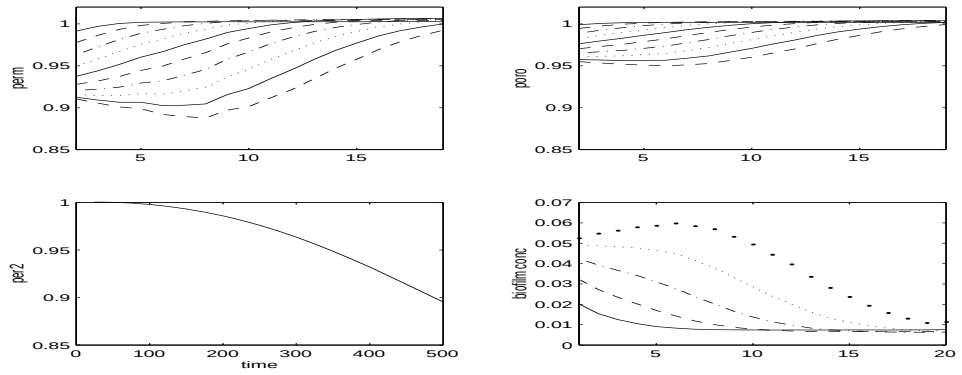

Figure 7: Porosity and permeability changes for case A for three dimensional simulations.

4.3 Case B: Effects of EPS Reaction Rates.

In case B we double the EPS reaction rates, k_1 and k_2, keeping other parameters fixed at their base-case values. We examine results for the three-dimensional simulations, shown in figures 8 and 9. As expected, we see higher concentrations of EPS than in the base case. We also see slightly lower concentrations of bacteria in the adsorbed phase, reflecting the fact that more nutrients are converted to EPS, leaving a lower concentration of nutrients available for conversion to bacteria. The simulations predict a greater decrease in permeability and greater diminution of nutrient concentrations.

Case B also reveals a curious result. While we expect higher concentrations of suspended EPS than in the base case, it may seem strange that there are also higher concentrations of suspended bacteria. To explain this result, note that biofilm concentrations are higher, which implies that

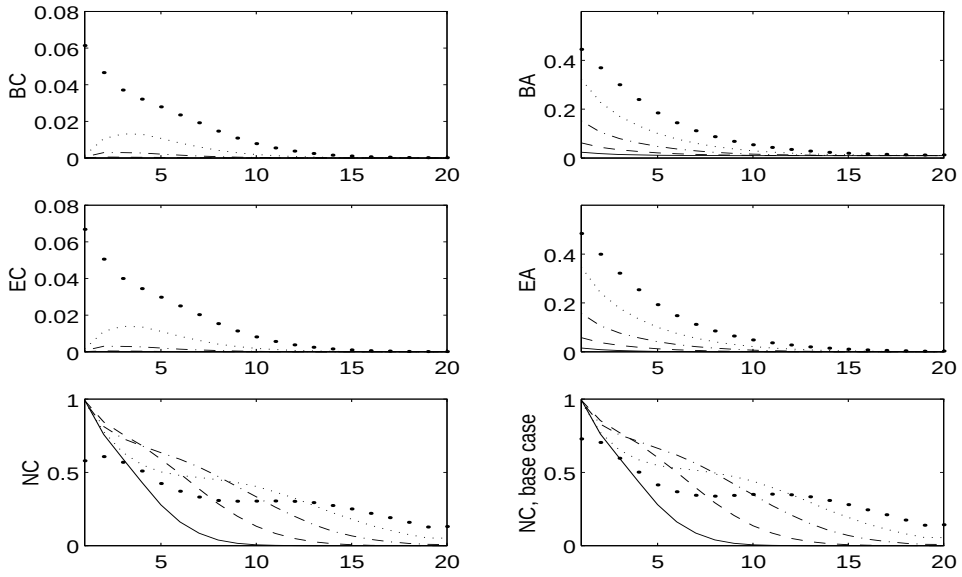

Figure 8: Concentration profiles for case B for three dimensional simulations. Case B has higher EPS reaction rate constants.

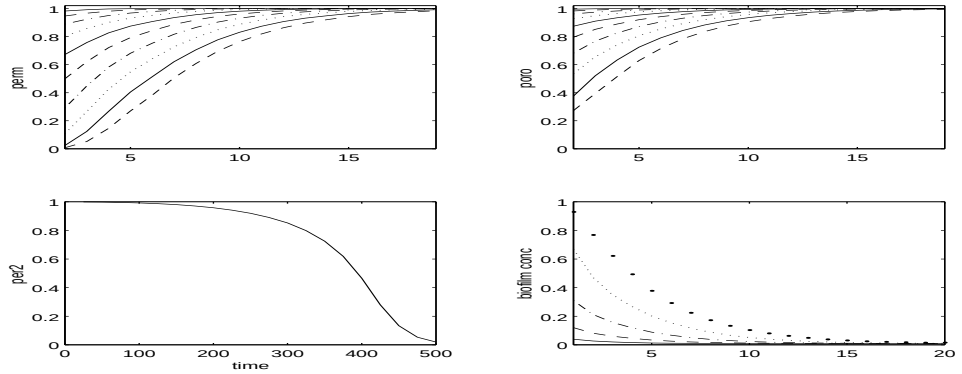

Figure 9: Porosity and permeability changes for case B for three dimensional simulations.

the biofilm layer is thicker, so total biomass erosion is higher. Most of the bacteria in solution have been sloughed from the biofilm.

4.4 Case C: Effects of Biomass Production in the Fluid.

Case C illustrates what happens when bacteria and EPS are produced mainly in solution, rather than in the biofilm, and when the biofilm that does attach is easily eroded. This case contrasts with the base case and Case B, in which most of the bacteria and EPS growth occurs in the biofilm. To achieve greater growth in the fluid, we halve the value of μ_{B}, quadruple the value of μ_b, and increase k_E twenty-fold. Physically, this slows the reactions in the biofilm and enhances them in the fluid, at the same time permitting increased erosion. The results for the three-dimensional simulations appear in figures 10 and 11. More of the bacteria and EPS advect downstream, and

higher concentrations occur in the adsorbed phase than in case A. We attribute these effects to the fact that there are more bacteria and EPS in suspension, and their concentrations influence adsorption rates. Correspondingly, there is a larger permeability decrease than for case A, but the decrease is smaller than in the base case, where there is less erosion.

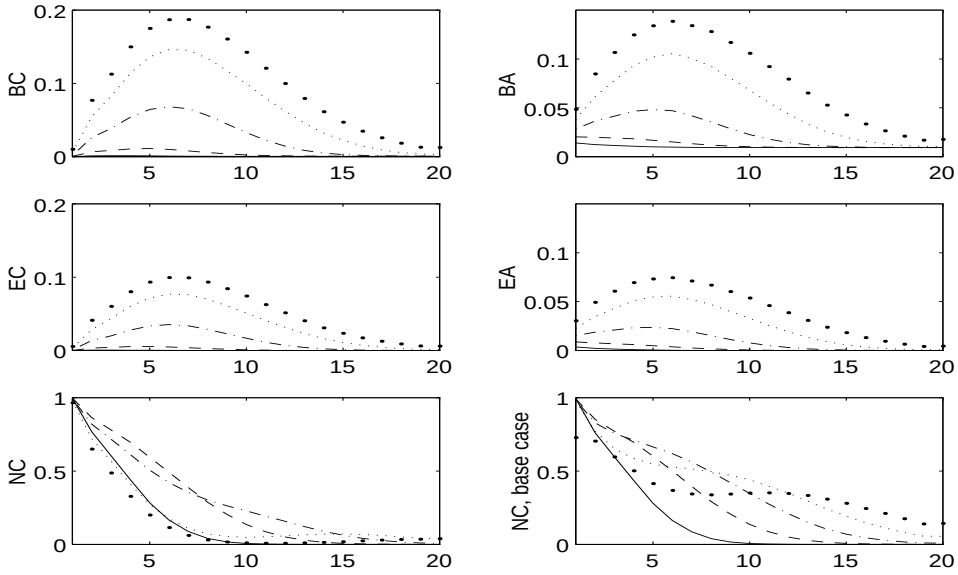

Figure 10: Concentration profiles for case C for three dimensional simulations. Case C has higher reaction rate constants in the solution phase and more erosion.

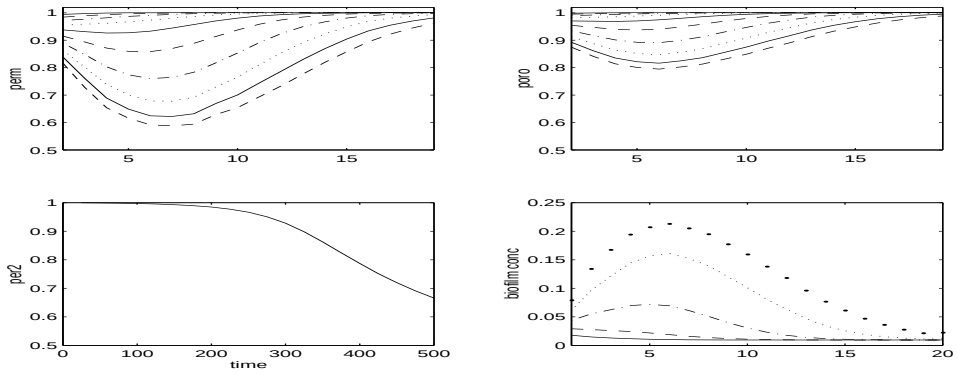

Figure 11: Porosity and permeability profiles for case C for three dimensional simulations.

4.5 Comparison Among Cases.

To compare the different cases, we examine mean concentration profiles and normalized permeability at the end of the simulations. Figure 12 shows values for the three-dimensional systems. Cases A and C both have higher erosion rates, so they both show higher concentrations of suspended bacteria and EPS than the other cases. In case C these concentrations are even higher, because

the reaction rate is higher in the fluid. In cases A and C the permeability reductions are greater near the middle of the network. In the base case the permeability reduction is much greater near the inlet. When erosion rates are small, bacteria tend to grow in place, and their populations grow fastest at the inlet, where nutrient concentrations are highest. The permeability reduction is relatively small for case A than for case C, owing to the smaller adsorption rate. Decreased adsorption also yields peak biomass concentrations further downstream.

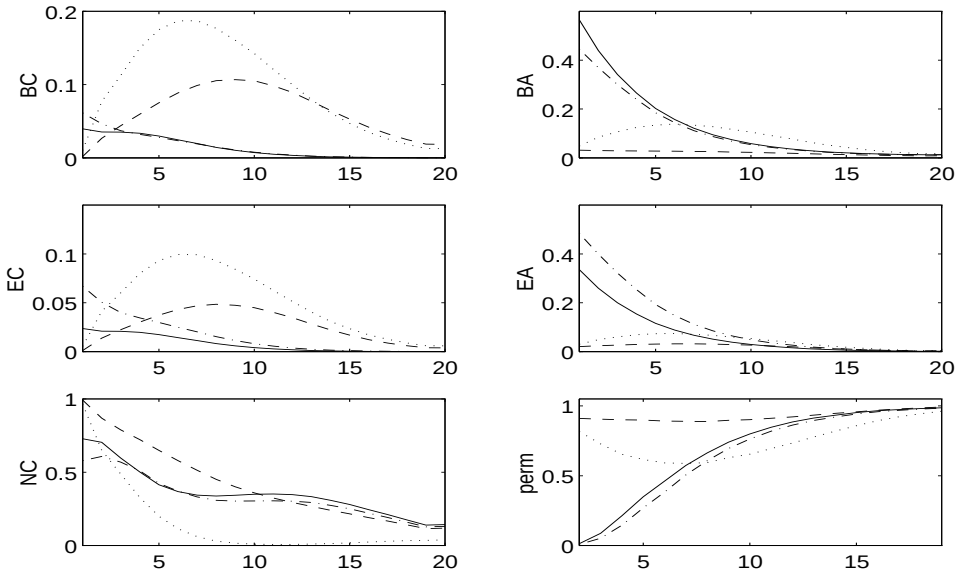

Figure 12: Comparison of concentration and permeability profiles at the end of three-dimensional simulations. — base; - - - A; –·–·– B; ··· C.

Case B is similar to the base case, except that bacteria and EPS concentrations are reversed in magnitude. This result reflects the fact that the reaction rate for EPS is higher in case B. Otherwise, there is little difference in permeability profiles between case B and the base case.

4.6 Removing Simplifications

The basic framework of this model can accommodate many additional processes. In this paper we present a simple version and investigate how a few parameters can affect the permeability of a porous medium. In this section, we discuss a few physical processes that we have neglected and suggest ways in which they may be incorporated into our model

We have been using one bacteria species and one nutrient species. This may be realistic in some lab-scale experiments, but in general there can be several species of bacteria and many components affecting growth of bacteria and EPS. Incorporating additional species into the model may be accomplished by lengthening the vectors $\mathbf{u}$ and $\mathbf{w}$ in section 3.2. There are also processes that we ignore, such as the death of bacteria cells and a concentration of nutrients required for subsistence of bacteria (Characklis and Marshall, 1990). These may be incorporated into the functions $\mathbf{f}_{1,r}$, $\mathbf{f}_{1,s}$, $\mathbf{f}_{2,r}$, and $\mathbf{f}_{2,s}$ in section 3.2.

We have constructed grids in two and three dimensions to represent an isotropic porous

medium. It would be possible to represent an anisotropic medium by assigning pipe radii from different probability distributions, depending on spatial orientation. We have also not used any geostatistics in assigning original pipe radii. We have included an erosion term in our model, but have completely ignored "sloughing" of large clumps of biofilm. In a pair of papers investigating two different bacteria strains, Vandevivere and Baveye (1992a,b) conclude in one case that EPS production is a major contributor to permeability reduction. In another case they observe that large aggregates blocking pores are an important clogging mechanism. Some type of random process could be used to slough clumps of biofilm from pore walls, perhaps dependent on shear stresses at the surface. Imdakm and Sahimi (1991) present an interesting method for determining the effect these clumps have on a network.

We have assumed that bacteria and EPS have the same density. This is not necessarily the case, and accounting for different densities would require a small change in how biofilm thickness is calculated. Two other simplifications are not as easy to rescind. We have assumed that the viscosity of the fluid is constant, and that pipe radius is the only factor affecting flow resistance in individual pipes. These two assumptions are suspect, and it will require care to incorporate variable viscosity and friction effects into the model.

4.7 Summary of Computational Results

These numerical results are consistent with the empirically known physics of the system:

- Higher reaction rates result in higher bacteria and EPS concentrations.
- Higher erosion rates tend to shift these biomass concentrations further downstream.
- Simulated permeability profiles agree well with published results of physical experiments.
- The numerics confirm the possibility of achieving significant permeability reduction using biofilms.

Of particular practical interest is the ability of the model to illustrate the effects that process parameters have on the location of biobarriers. Several of the cases examined suggest avenues for further experimentation to help translate these observations into process design principles.

5 Conclusions

The network model described in this paper simulates growth, adsorption, transport, and erosion of bacteria and EPS in porous media. The model allows one to observe computationally how various process parameters affect the flow properties of a medium. By averaging over the network and over ensembles of realizations, one can upscale phenomena occuring at the microscopic scale — such as the constriction of pores by biofilm — to obtain macroscopic effects — such as permeability reduction and the formation of biobarriers.

Although the method yields qualitatively similar results for two- and three-dimensional networks, the results are quantitatively different in these two settings. Therefore, practical calculations require three space dimensions. An interesting direction for further work is to examine

whether earlier notions, asserting that macroscopic flow properties are insensitive to network geometry, remain valid when the flow is coupled to processes that alter the medium.

The results of simulations reported here are physically reasonable, and they compare well, qualitatively, with experiments. Specifically, computed results for the base case and for cases B and D qualitatively match permeability reductions reported by Vandevivere and Baveye (1992) and Taylor and Jaffé (1990). Numerical simulations offer two advantages over experiments: They take tens of minutes to perform, and they allow one to interrogate a model "soil column" anywhere along its length. Thus, while the model certainly does not obviate laboratory work, it can help narrow the selection of process design experiments that may take months to perform in vitro.

Perhaps the main value of the model is as a tool for upscaling relationships among biofilm concentrations, porosities, and permeabilities. These relationships are essential for accurate models of biofilm effects at the continuum scale.

6 References

1. Alexander, M., 1994, Biodegradation and Bioremediation, Academic Press.

2. Amy, P. S. and Haldeman, D. L., editors, 1997, Chapter 17: "Biofilm Processes in Porous Media — Practical Applications," The Microbiology of the Terrestrial Deep Subsurface, CRC Press LLC.

3. Bakke, R., Trulear, M. G. and Characklis, W. G., 1984, Activity of Pseudomonsa aeruginosa in Biofilms: steady-state, *Biotechnology and Bioengineering*, **26**, 1418-1424.

4. Characklis, W. G. and Marshall, K. C., editors, 1990, Biofilms, John Wiley & Sons, New York, 796 pages.

5. Escher, A. R., 1986, Colonization of a Smooth Surface by Pseudomonas aeruginosa: Image Analysis Methods, Ph.D. Dissertation, Montana State University, Bozeman, MT.

6. Imdakm, A. O. and Sahimi, M. 1991, Computer Simulation of Particle Transport Processes in Flow Through Porous Media, *Chemical Engineering Science*, **46**, (8), 1977-1993.

7. Jerauld, G. R., Hatfield, J. C., Scriven, L. E., and Davis, H. T., 1984a, Percolation and Conduction on Voronoi and Triangular Networks: A Case Study in Topological Disorder, *J. Phys. C: Solid State Phys.*, **17**, 1519-1529.

8. Jerauld, G. R., Scriven, L. E., and Davis, H. T., 1984b, Percolation and Conduction on the 3D Voronoi and Regular Networks: A Second Case Study in Topological Disorder, *J. Phys. C: Solid State Phys.*, **17**, 3429-3439.

9. Koplik, J., 1982, Creeping Flow in Two-Dimensional Networks, *J. Fluid Mech.*, **119**, 219-247.

10. Lindqvist, R., Cho, J. S., and Enfield, C. G., 1994, A Kinetic Model for Cell Density Dependent Bacterial Transport in Porous Media, *Water Resources Research*, **30**(12), 3291-3299.

11. MacLeod, F. A., Lappin-Scott, H. M. and Costerton, J. W., 1988, Plugging of a Model Rock System by Using Starved Bacteria, *Applied and Environmental Microbiology*, **54**,(6), 1365-1372.

12. Melo, L. F., Bott, T. R., Fletcher, M., and Capdeville, B., editors, 1992, Biofilms - Science and Technology, Kluwer Academic Publishers, The Netherlands, 708 pages.

13. Mitchell, R., 1978, Water Pollution Microbiology, Volume 2, John Wiley & Sons, New York, 442 pages.

14. Scheidegger, A. E., 1957, The Physics of Flow Through Porous Media, University of Toronto Press.

15. Suchomel, B. J., Chen, B. M. and Allen, M. B., Network Model of Flow, Transport and Biofilm Effects in Porous Media, to appear in *Transport in Porous Media.*

16. Taylor, S. W., and Jaffé, P. R., 1990, Biofilm Growth and the Related Changes in the Physical Properties of a Porous Medium 1. Experimental Investigation, *Water Resources Research*, **26**,(9), 2153-2159.

17. Vandevivere, P., and Baveye, P., 1992a, Effect of Bacterial Extracellular Polymers on the Saturated Hydraulic Conductivity of Sand Columns, *Applied and Environmental Microbiology*, **58**, (5), 1690-1698.

18. Vandevivere, P., and Baveye, P., 1992b, Saturated Hydraulic Conductivity Reduction Caused by Aerobic Bacteria in Sand Columns, *Soil Science Society of America Journal*, **56**, (1), 1-13.

19. Wanner, O. and Gujer, W., 1986, A Multispecies Biofilm Model, *Biotechnology and Bioengineering*, **28**, 314-328.

A Parameters used in simulations

Blank entries correspond to values equal to those in the 3-D base case.

	3-D base	2-D base	A	B	C
μ	1				
σ	0.6				
flowrate, Q	70	35			
Y_B	0.4				
Y_b	0.4				
Y_E	0.6				
Y_e	0.6				
k_1	0.5			1.0	
k_1'	0.002				
k_2	0.5			1.0	
k_2'	0.002				
μ_B	0.02				0.01
μ_b	0.02				0.08
K_s	1				
k_E	0.005		0.5		0.1
k_e	0.01				
k_b	0.01		0.002		
$c_{n,\text{in}}$	1				
B_o	0.01				
ρ_B	1				
$N_{c,min}$	4				
$N_{c,max}$	5				
B_o	0.01				
# simulations	20				